Altitude-compensating axisymmetric supersonic nozzle design and flow analysis

Sidali HAIF*,[1], Hakim KBAB[1], Amina BENKHEDDA[1]

*Corresponding author
[1]Aeronautical Sciences Laboratory (LSA), Aeronautics and Space Studies Institute, Blida 1 University BP270 Soumaa street, Blida, Algeria,
haif.sidali@etu.univ-blida.dz*

DOI: 10.13111/2066-8201.2023.15.2.4

Received: 25 February 2023/ Accepted: 06 April 2023/ Published: June 2023

Abstract: *Altitude-adapted nozzles are designed to facilitate flow adaptation during rocket ascent in the atmosphere, without requiring mechanical activation. As a consequence, the performance of the nozzle is significantly improved. The aim of this study is to develop a new profile of axisymmetric supersonic nozzles adapted at altitude (Dual Bell Nozzle with Central Body), which is characterized by an E-D nozzle as a basic profile. The performances obtained for this nozzle (E-D Nozzle) are then compared to those of a Plug nozzle. The E-D nozzle shows significant performance advantages over the Plug nozzle, including a 13.02% increase in thrust, knowing that the length of the E-D nozzle is half that of the Plug nozzle under the same design conditions. Finally, viscous calculations using the k-ω SST turbulence model were conducted to compare the performance of the dual bell nozzle with central body (DBNCB) and the E-D nozzle with the same cross-sectional ratio, and to assess the impact of nozzle pressure ratio (NPR) variations on the operation mode of the DBNCB. The results obtained show that the DBNCB offers the best performance in most phases of flight.*

Key Words: *E-D nozzle, Dual bell nozzle, ANSYS-Fluent, Method of characteristics (MOC), FORTRAN*

1. INTRODUCTION

Researchers have been designing innovative aerospace propulsion nozzles to enhance performance, challenged by international competition and the search for greater performance. The primary objective behind this design is to enhance the nozzle's performance in non-design working conditions such as Sea-Level mode and High-Altitude mode. At low altitudes, particularly during take-off and in the early stages of the trajectory, increased atmospheric pressure from the ground results in the formation of a Mach disk and shocks within the divergent part of the nozzle, which causes flow separation in the nozzle. The inherent asymmetry of separation in the divergent results in side loads that size the system while penalizing the payload. Consequently, there is a decrease in efficiency, and on the other hand, at higher altitudes, atmospheric pressure decreases, causing the exit jet to continue to expand beyond the nozzle exit (under-expansion). This external expansion does not exert any force on the nozzle wall, and this is what affects the thrust. Therefore, this again decreases the efficiency of the nozzle. In order to avoid all this lack of performance in the two modes of operation, the researchers explored the concept of self-adaptation. One of the most important nozzles working on this concept is the dual bell nozzle. At low altitudes and at high exit

pressures, the first part of the profile ensures flow expansion. Then, when the external pressure decreases following a specific transition at high altitude, the two parts of the divergent work together in tandem to ensure the expansion of gases in the nozzle. This concept, on the one hand, should increase the propulsion performance of the engine and, on the other hand, at low altitudes, should stabilize the separation in the divergent around the junction point of the profile. The dual bell nozzle has a fractional divergence at a point of inflection, which in turn acts to force the flow to separate from the wall of the nozzle, and this is to increase the thrust of the launcher at low altitude. The inflection of the nozzle contour ensures a symmetrical and controlled flow separation. In the first mode of operation (low altitude), the inflection of the nozzle ensures symmetrical and controlled separation. This is what limits the production of high side loads, in contrast to conventional nozzles (see Fig. 1a).

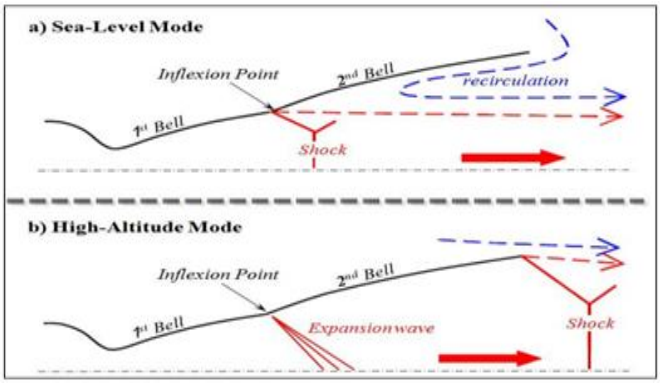

Fig. 1 – Main operating modes of a dual bell nozzle

After the transition and in the second mode of operation (high altitude), the cross section increases due to the expansion of the jet and clinging to the wall of the second profile. This leads to an improvement in the performance of the nozzle (see Fig. 2b).

The idea of using a dual bell nozzle to improve performance was first introduced by Clowles and Foster in 1949, and was later patented by Rocketdyne in the 1960s [1, 2, 3]. However, it wasn't until the 1990s that research on dual bell nozzles gained attention due to the development of computational fluid dynamics (CFD) technology. In 1994, Rocketdyne and the European Space Agency (ESA) conducted tests on dual bell nozzles, and found that they provided 12.1% more thrust than conventional CD nozzles. Since then, numerous studies have been conducted to optimize design variables such as the angle of inflection and the contour of the extension. In the 2000s, various experiments and numerical studies were carried out in the US and Europe, with a focus on optimizing transitional behavior between the two operating modes of the nozzle. In 2015, Davis et al. developed a dual bell nozzle profile design process for application on the Nanolaunch 1200 [3]. In the same year, Schneider and Génin conducted a numerical study on the effect of feeding pressure gradients and turbulence models on the flow transition in the dual bell nozzle. Several studies have also been conducted on the design method and performance evaluation of these nozzles [4]. Hamitouche et al. studied the design of dual bell nozzles using the indirect method of characteristics in 2017 [5]. Schneider et al. conducted a numerical study to investigate the effect of a film-cooled dual bell nozzle extension on the transition between two operating modes.

Therefore, they performed unsteady Reynolds-averaged Navier-Stokes simulations of the transition process. The cooling fluid (hydrogen gas) is injected upstream of the inflection point of the dual bell nozzle. They concluded that increasing coolant mass flow rate and propellant

mixing ratios leads to a gap in the dual bell nozzle transition pressure ratio at lower values that leads to active control of the transition from the dual bell mode of operation [6].

In 2020, within the Control and Computer Engineering Department of the Politecnico di Torino, work was carried out by Ferrero et al. on the control of the transition in a dual bell nozzle using CFD [7].

The control is based on the injection of a secondary flow in the region close to the point of inflection. The results show that the injection of a secondary flow in the radial direction makes it possible to increase the transitional NPR.

For the first time, the influence of external flow on the flow of the nozzle and its transition from sea level to high altitude mode are discussed by Bolgar et al. [8]. They made experimental measurements on a dual bell nozzle with transonic and supersonic external flows around a launcher-type forward body.

This study was carried out in the Trisonic wind tunnel in Munich. The researchers proposed a new definition for the nozzle pressure ratio design criterion, which takes into account the significant pressure drop caused by a Prandtl-Meyer expansion around the nozzle lip in supersonic external flow conditions.

In recent times, Kbab et al. designed the profile of a dual bell nozzle using the direct method of characteristics.

They present a test case used to validate their calculation models which will be used to optimize the profile of a dual bell nozzle [9].

In our study, we aim to use the method of characteristics (MOC) [10] and the Prandtl-Mayer function to create new contours for the axisymmetric dual bell supersonic nozzle, and investigate the behavior of fluid parameters (such as Mach number and static pressure) along the nozzle walls.

This new nozzle is referred to as the Dual Bell Nozzle with Central Body (DBNCB), and features a central body and a double curved external wall that aids in straightening the flow. To define the nozzle contour, a calculation code was developed at the Aeronautical Sciences Laboratory (LSA). Furthermore, a numerical simulation of the flow using the Ansys-Fluent environment was conducted for our DBNCB nozzle and compared with an E-D nozzle with the same section ratio to test the performance of the two nozzles under different operating conditions.

2. DESIGN METHOD FOR A DBNCB CONTOUR

Consider that the fluid is an ideal gas during our work. The design of the DBNCB is made in two parts:

2.1 Design method for a DBNCB contour

In this study, we had a new idea in the field of dual bell nozzles: the replacement of the basic nozzle, which is a nozzle of the type (TIC, TOC,...), by an E-D nozzle. So the new BDNCD has an E-D nozzle as a basic nozzle. For the design of the basic nozzle profile, we have developed a program in FORTRAN.

This program is inspired by the program that designs the contour of the Plug nozzle [11] with changes in parameters and principle.

The approximate design method is based on simple wave flow concepts, which are described by T. L. Deynoud [11] (Fig. 2 and 3). The program described in this report is simple. It provides a diagram for designing the E-D nozzle contour diagram from the Prandtl-Meyer relation.

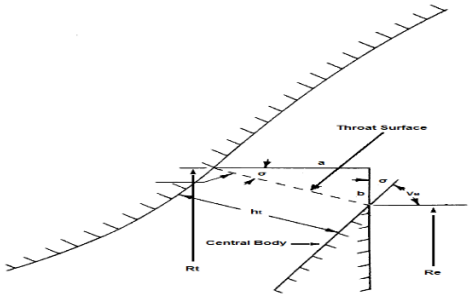

Fig. 2 – Throat nozzle configuration

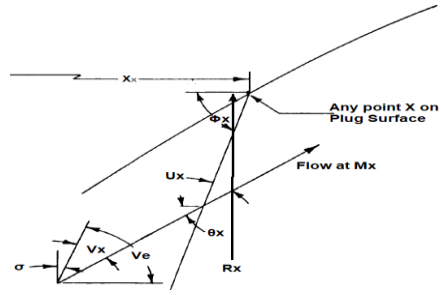

Fig. 3 – E-D Nozzle

To generate the basic nozzle profile, geometric data were needed, in our case: the application was made for a nozzle with a design Mach number $M_d = 3{,}4$. This nozzle is characterized by a central body radius $R_e = 2{,}0\ mm$ as well as by exit radius $R_b = 4{,}0\ mm$. Total pressure and total temperature are: $P_0 = 1200000\ Pa$ and $T_0 = 300\ K$, respectively, and the atmospheric pressure P_a is taken equal to $0{,}015P_0$.

Figure 4 presents the profile of the E-D nozzle produced by our computer code. The length of the base nozzle obtained $X_{L1} = 6{,}4\ mm$.

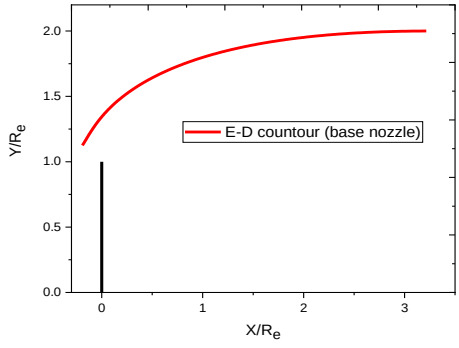

Fig. 4 – E-D Nozzle profile

Figure 5 presents the comparison of the Mach number on the wall between the numerical simulation (Fluent) and our program (FORTRAN), and Fig. 6 shows the wall pressure ratio.

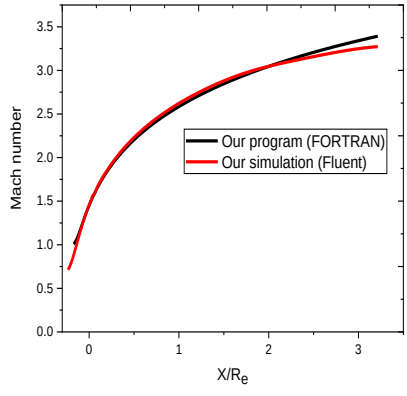

Fig. 5 – Wall Mach evolution

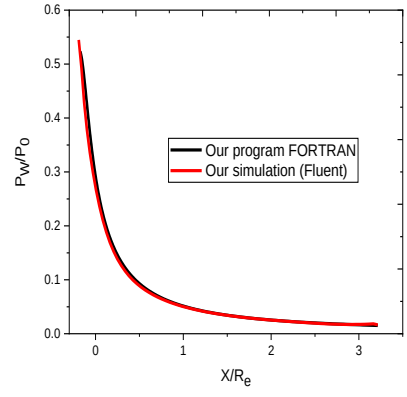

Fig. 6 – Wall pressure evolution

According to Fig. 5, the wall Mach number develops in two phases. In the initial phase, it increases very rapidly, close to the expansion zone, to reach a value of 2.1. In the second phase, a slower progression is observed in the divergent until the wall Mach value has reached the design Mach value at the end of the nozzle. For static wall pressure, the inverse occurs, as we notice a significant decrease in pressure at the initial phase, where the pressure value reaches $P_w = 0{,}083P_C$, and at the second phase, the pressure continues to decrease slightly until it reaches the value of the atmospheric pressure (see Fig. 5). Regarding this slight pressure drop in the second phase, Kbab et al. use a method to reduce the weight of the nozzle without significant impact on the thrust; this is done by truncating the nozzle in the second phase to a point where the best compromise (weight/performance) is respected [12]. They concluded that if an axisymmetric nozzle is truncated at 79% of its ideal length, we obtain a nozzle with a weight gain equal to 20.85% and a thrust loss equal to 0.987% only.

We also note a complete agreement between the results obtained by simulation (Fluent) and those calculated by the program (FORTRAN) for the parameters on the wall.

Figure 7 shows the Iso-Mach contours obtained by our simulation. Note that the Mach number in the throat is slightly supersonic, then increases until it reaches a value close to the design Mach value at the exit of the nozzle.

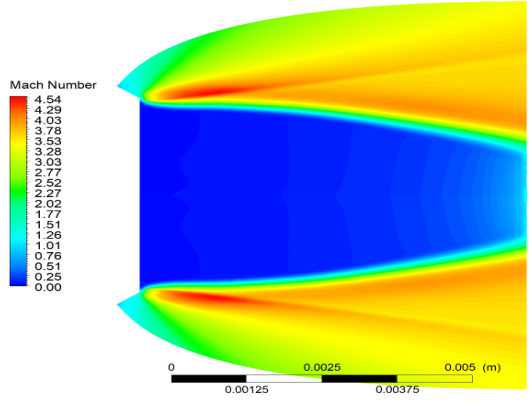

Fig. 7 – Iso-Mach contours

Figure 8 shows the Iso-Pressure contours for an E-D nozzle that operates within the design Mach number obtained by our simulation; the figure shows the Prandtl-Meyer expansion around the lip. Because there are no perturbations or pressure fluctuations, the flow in the E-D nozzle is typical isentropic along the divergent.

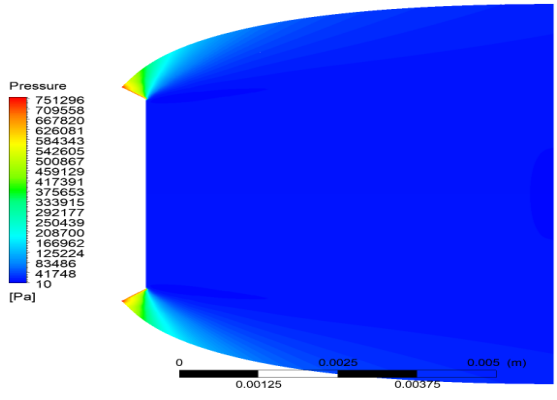

Fig. 8 – Iso-Pressure contours

Without the use of controlled flow separation mechanisms, the ED's nozzle adapts to each altitude. The ambient pressure regulates the nozzle's exit region in the open wake mode (Fig. 9), and the exhaust gas does not completely fill the nozzle. It should be superior to the majority of other advanced nozzles in this regard, with the exception of the plug nozzle [13]. In closed wake mode (Fig. 10), the entire exit area of nozzle is filled by the exhaust gases. The ambient pressure at which the transition of wake takes place from open to closed modes is known as the design pressure. If the ambient pressure is further decreased, then the remaining expansion would occur outside the nozzle just like a bell nozzle and in that case there is no benefit of altitude compensation.

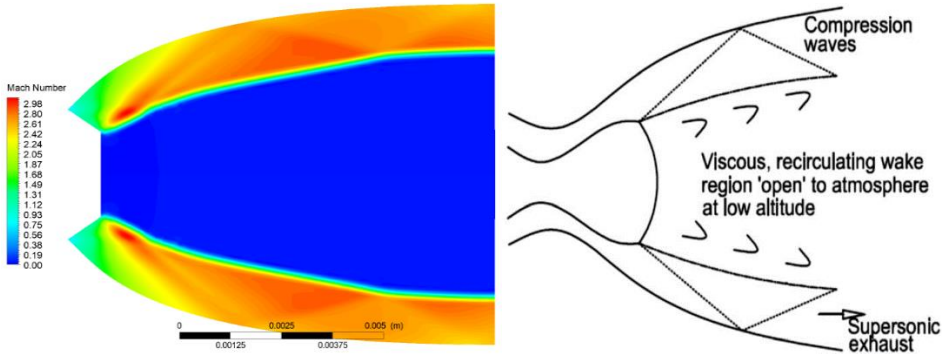

Fig. 9 – Iso-Mach contours (NPR=40)

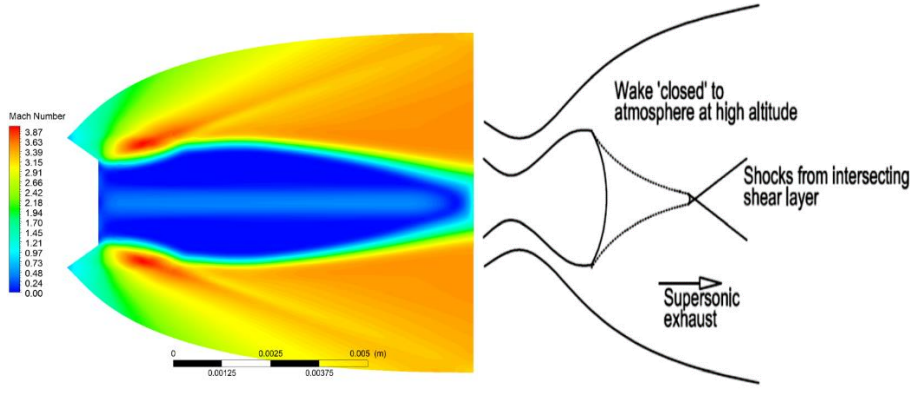

Fig. 10– Iso-Mach contours (NPR=320)

2.1.1 Comparison with a Plug nozzle

For the comparison between the two nozzles (E-D and Plug), the two nozzles must be built with the same section ratio and simulation condition (see Table 1).

Table 1 – Comparison of thrust and area

	E-D and Plug Nozzle
Total pressure (Pa)	150000
Static pressure (Pa)	79242
Ambient pressure (Pa)	2268.75
Design Mach Number	3.40

The exit section of the two nozzles equals $1300\ mm^2$, and to obtain an E-D nozzle with this section, it is necessary to choose $R_e = 15\ mm$ and $R_b = 25\ mm$.

Figure 11 shows the comparison of the E-D nozzle with the Plug nozzle for the same design conditions (Mach, Exit section).

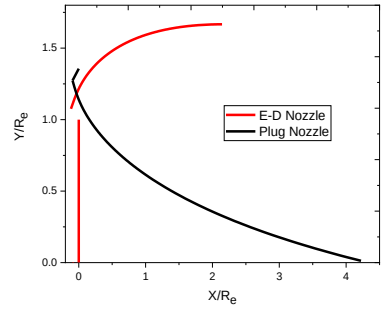

Fig. 11 – The profiles of the E-D and Plug nozzles for $Mach = 3{,}4$

The length of the Plug nozzle is $63.3\ mm$, while the length of the E-D nozzle is $32.1\ mm$. We conclude that the E-D nozzle length is equal to half the Plug nozzle length for the same design condition. So the E-D nozzle is less encumbered.

Figures 12 and 13 represent the pressure and Mach evolution of the wall $Mach = 3{,}4$., for the two nozzles (E-D and Plug), respectively.

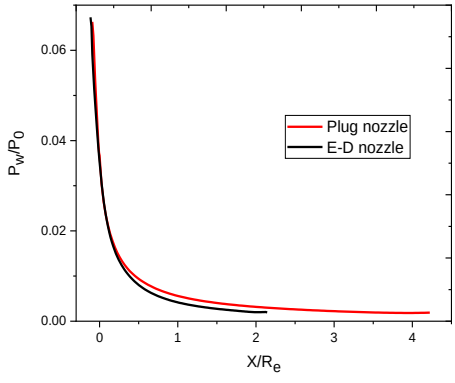

Fig. 12 – Pressure ratio variations

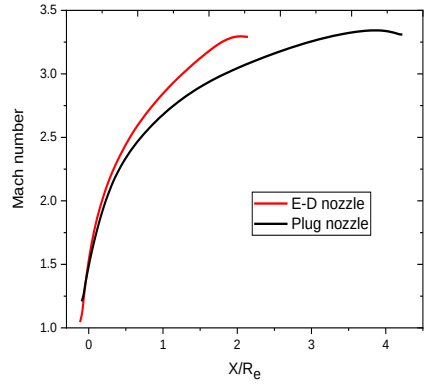

Fig. 13 – Mach number variations

For the evolution of pressure on the walls of the two nozzles (Fig. 12), it is noted that the pressure drop and its attainment of the required value are faster in the case of the E-D nozzle. It is the same for the increase in the Mach number (see Fig. 11). For comparison, we calculated the pressure thrust using the following function: $\int (P_x - P_a)dA$. From Table 2, we see a thrust increase of 13.02% for the E-D nozzle compared to the Plug nozzle.

Table 2– Comparison of thrust and area

	E-D Nozzle	Plug Nozzle
Area (m2)	0.00518	0.00286
Thrust (N)	43.41388	37.76218

After this great superiority of the E-D nozzle over the Plug nozzle in terms of performance and size, there is another advantage, which is the possibility of adding a secondary extension (geometric advantage). We will discuss this in the second part of this study.

2.2 Design of the second bell (nozzle extension)

The contour of the nozzle extension (second bell) is designed to give a constant wall Mach number M_2. This is done by applying the characteristics method to the Prandtl-Meyer expansion around junction point *J* with equal intensity $\frac{M_2}{M_1}$ (see Fig. 14) for the inviscid fluid hypothesis.

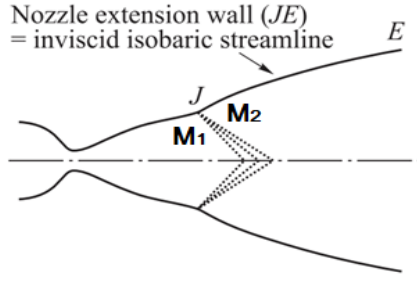

Fig. 14 – Centered expansion at junction J [14]

To generate the second bell, we only need the data for the first bell and the second curve because the second contour is only the extension of the first contour. The data for the first bell (base nozzle) design is shown in Table 3.

Table 3 – Data for the design of the first bell

M_d (Design Mach number)	3.9
R_e (Center body radius)	5.0 mm
R_b (Exit radius)	17.4 mm

For our case, the basic nozzle profile is obtained by truncating an E-D ideal nozzle. The Mach number at the exit of the truncated nozzle equals $M = 3.4$ with a length of $X_t = 25.1\ mm$ and an exit radius $R_t = 16{,}6\ mm$. For the second bell design data, we have:

A second Mach number M_2, thus the second contour length X_{L2}. For our case, we take $M_2 = 5.3$ and $X_{L2} = 72.3\ mm$.

Figure 15 represents the DBNCB profile obtained by our FORTRAN program. The junction point coordinates *J* (where the two profiles meet) are given by $X_J = 25.1\ mm$ and $Y_J = 16.6\ mm$. The total nozzle length is $L_T = 97.4\ mm$. The exit radius of the nozzle is $R_T = 36.4\ mm$.

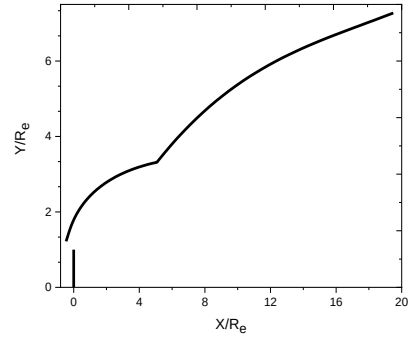

Fig. 15 – DBNCB profile

Figure 16 represents the distribution of the wall pressure (simulation and program) on the dual bell nozzle with central body. Pressure begins to decrease rapidly in the initial expansion zone in the vicinity of the pass until its value reaches $P_W = 17968\ P_a$ at junction J. Then a Prandtl–Meyer expansion fan is apparent. It causes a sudden drop in pressure in the wall to the value of $P_W = 1609\ P_a$. Beyond the junction point, the wall pressure remains constant along the second bell. It is noted that there is an excellent match between the results obtained by the Fluent simulation and those obtained by the FORTRAN program.

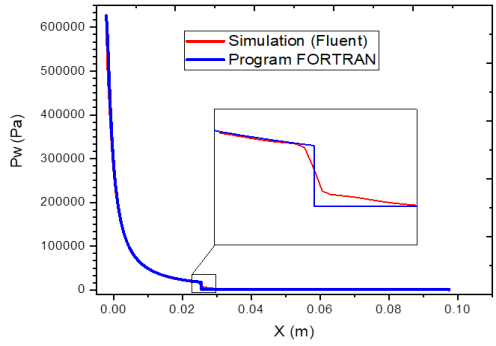

Fig. 16 – DBNCB wall pressure profiles

Figure 17 illustrates the Mach contour in the DBNCB for an inviscid Euler calculation by the ANSYS-Fluent code.

In Fig. 17, there is no internal shock formation; instead, two Prandtl-Meyer expansion fans are visible with the lip and inflection point of this nozzle.

The Prandtl-Meyer expansion usually occurs when a supersonic flow deviates from the curvature of the wall. We also note that the flow is perfectly attached to the walls of the nozzle (the absence of flow separation).

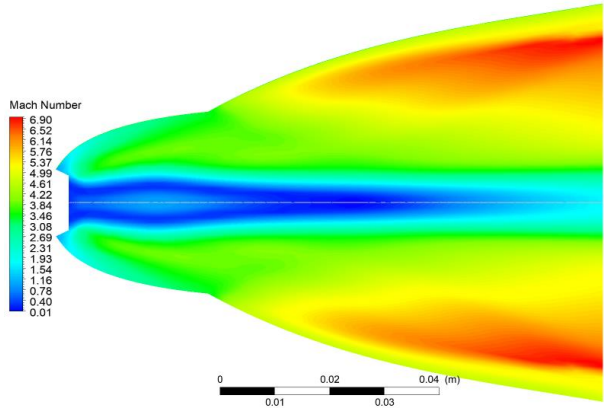

Fig. 17 – Iso-Mach contour of a DBNCB

3. VISCOUS CALCULATIONS

The best tool to test our designs is numerical simulation software. With simulation software, calculations are extremely accurate and can take into account many parameters for a very reliable study of our designs.

Among the tools widely used by researchers and industrialists is the Fluent code. The numerical simulation of the viscous flow is carried out in Fluent. They solve the Navier-Stokes

equations with a RANS (Reynolds Averaged Navier Stokes) approach. To model the Reynolds stresses that appear in the equations, various turbulence models can be used.

Two models were tested during the study: the Spalart-Allmaras model and the k-ω SST model. Figure 18 depicts the calculated wall pressure in inviscid flow, turbulent viscous flow (Spalart-Allmaras and k-ω SST), and by the characteristics method at the junction point of a DBNCB operating in high altitude mode. The k-ω SST model and the non-viscous calculation (Euler) have very good consistency.

This validates the k-ω SST turbulence model's ability to predict flow near the wall. It should also be noted that k-ω SST is a new model that combines the benefits of k-ω near the wall and k-ε far from the body.

We chose the k-ω SST turbulence model for this study because we needed more precision near the wall.

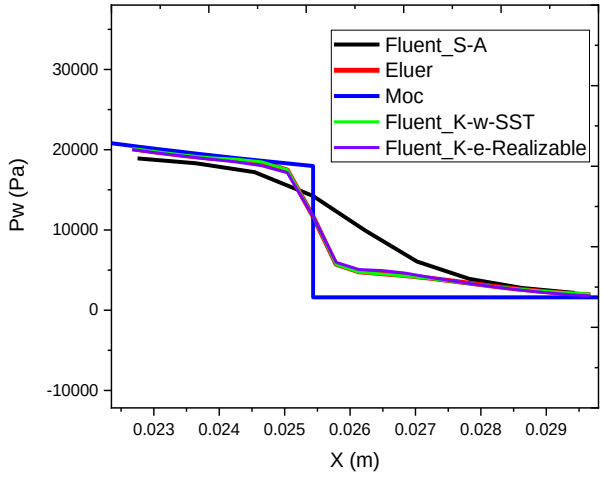

Fig. 18 – The wall pressure at the junction point *J*

3.1 The influence of the mesh

The choice of the mesh is a major step in a numerical simulation. After creating the geometry, it is very important to choose a suitable mesh to deal with the problem.

To illustrate the importance of the mesh, we tested three meshes of different resolutions. A mesh A composed of 10342 cells and a mesh B composed of 107100 cells. The last C mesh generated with 150002 cells.

The distribution of the pressure on the walls is almost the same for the three meshes, except for mesh A (see Fig. 19), where there is a difference.

Meshes B and C generate similar results for the pressure on the walls (the number of nodes does not really affect the solution). The computation times of the 3 meshes are very different.

It is obvious that the very refined mesh will take a lot more resources, memory, and CPU time for the calculation. However, in our situation, it is essential to have this precision to be able to visualize the phenomenon.

Therefore, it will be a matter of choosing the models well to save calculation time. Convergence problems can occur when choosing a coarse mesh. Therefore, mesh B is chosen for the present study in order to reduce the computation time.

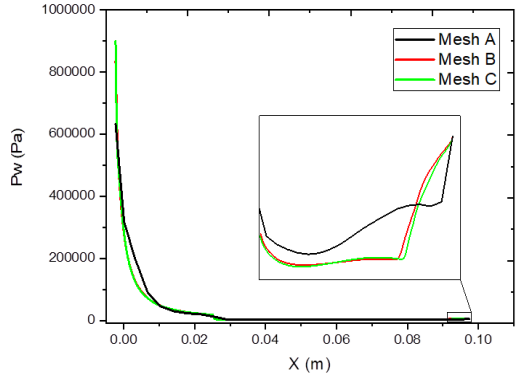

Fig. 19 – Pressure distribution of wall for DBNCBB at NPR = 266 with different mesh

The characteristics of the calculation solver used for the analysis of the DBNCB are as follows:

1. The baseline solver was selected as a double-precision Density-based coupled solver with Implicit Time Integration.
2. For spatial discretization "Least squares cell-based" was used in which the solution was assumed to vary linearly.
3. For the interpolation of the values of pressure, momentum, turbulent kinetic energy, specific dissipation rate and energy second-order upwind scheme was used.
4. To calculate the viscosity of air the Sutherland equation is used.
5. Numerical analysis was performed under stable conditions. Initialization for the steady-state problem was performed using full multigrid (FMG) initialization to obtain the initial solution, and the inlet boundary condition was provided to give the reference value.

Figure 20 illustrates the mesh and the boundary conditions adopted. During the current viscous calculations, the ambient conditions around the DBNCB were modeled by applying a calculation domain of $300R_e$ in the x direction, and $150R_e$ in the y direction, with R_e representing the throat radius

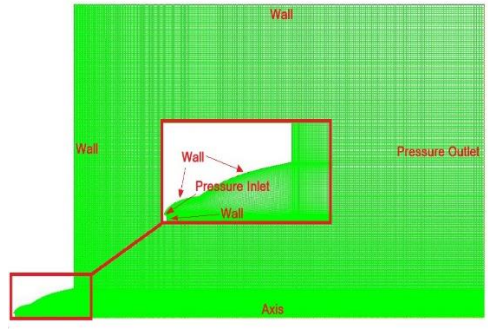

Fig. 20 – Numerical computation domain, boundary conditions and adopted nozzle grid

The observation of the pressure at the level of the wall of the nozzle makes it possible to understand the flow inside this nozzle. Figure 21 shows the evolution of the wall pressure along the wall of the DBNCB in high altitude mode. The result obtained by the numerical method (MOC calculation) is compared with those of the non-viscous simulations and the viscous simulation (k-ω SST). All the curves show an isentropic expansion in the first bell (E-D nozzle). At the junction point between the first and second bells, a drop in pressure is

observed. This can be explained by the presence of a Prandtl-Meyer expansion caused by the inflection of the nozzle profile.

In extension (second bell), all the curves become constant until the exit of the nozzle. This result reveals the good design of the DBNCB profile geometry.

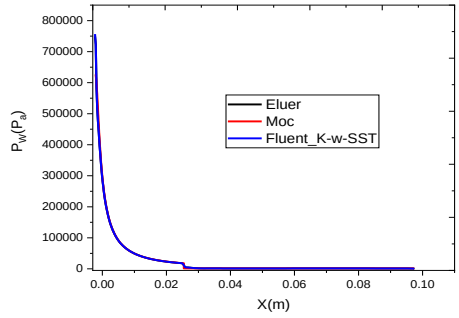

Fig. 21 – Comparison between the wall pressure calculated by MOC and numerical simulations

3.2 NPR's influence

In order to study the influence of the variation of the nozzle pressure ratios (NPR) on the mode of operation of the DBNCB, we performed several nozzle simulations in different operating modes by switching from Sea-Level Mode (Fig. 22 and 23), Transition Mode (Fig. 24) to High-Altitude Mode (Fig. 25).

The wall pressure variation according to NPR is shown in Fig. 26. In order to accurately reproduce the physics of the studied problem, the gauge total pressure was kept constant while the ambient pressure was changed (see Table 4).

Table 4 – boundary conditions values

	DBNCB
Gauge Total Pressure (Pa)	1200000
Supersonic/Initial Gauge Pressure (Pa)	633300
Total Temperature (K)	330
Pressure outlet (Pa)	Different NPR

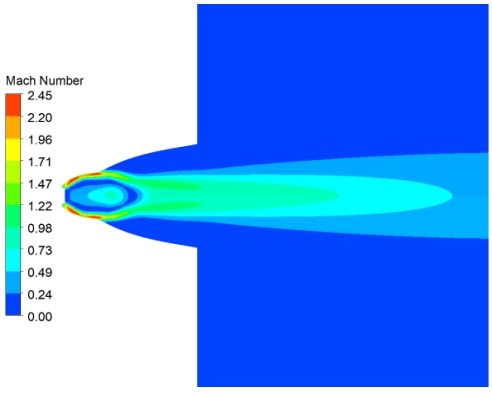

Fig. 22 – Mach number distribution at Sea-Level Mode NPR=10

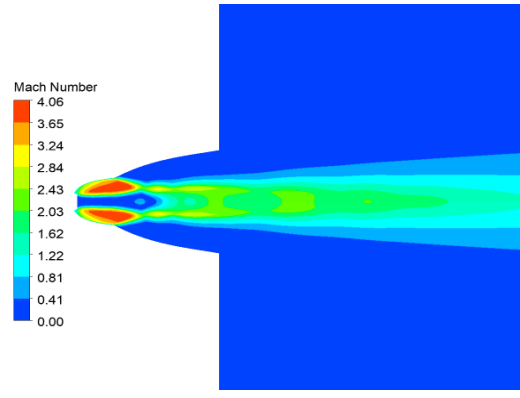

Fig. 23 – Mach number distribution at Sea-Level Mode NPR=30

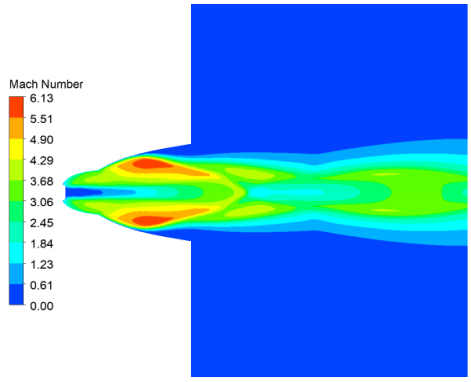

Fig. 24 – Mach number distribution in Transition Mode NPR=150

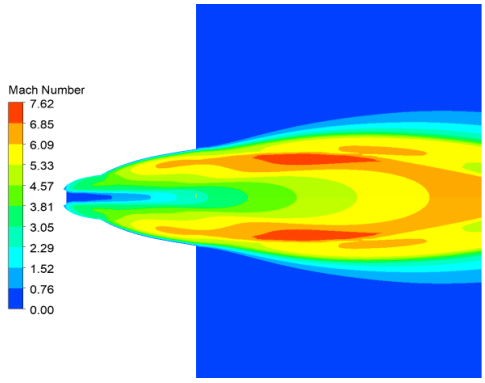

Fig. 25 – Mach number distribution at High-Altitude Mode NPR=900

According to the results of the figures, the nozzle operates in low altitude mode (Sea-Level Mode) for NPR ≤ 30, a brutal increase in wall pressure after the inflection point. It can be seen that the separation point remains stable at the inflection point of the nozzle. This reduces the side load in low altitude mode. In the case of NPR between 80 and 400, it is noted that the separation point ramps along the extension wall of the nozzle. Consequently, the nozzle operates during this phase in transition mode. We note that for NPR=900, the nozzle operates in High-Altitude mode.

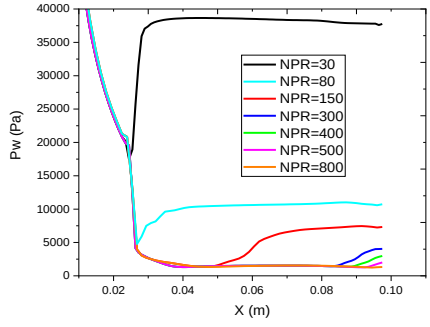

Fig. 26 – Wall pressure distribution for different values of NPR

3.3 Comparison between DBNCB and ED nozzle

In this section, the DBNCB is compared to the ED nozzle, which has the same area ratio. The weight and thrust of the two nozzles are compared. All geometries are studied under similar boundary conditions.

After comparing the profiles of the DBNCB and the E-D nozzle, as indicated in Fig. 27 and Table 5. It has been noted that the length of the DBNCB is 97.40 (mm) and the length of the E-D nozzle is 177.56 (mm) for the same section ratio $\frac{A_t}{A_e} = 0.87$, so there is a decrease in length of 45.15%. As a result, the DBNCB is less cluttered. To express the weight, the surface area of each of the two nozzles is calculated, where the surface area of the E-D nozzle equals $0.035\ m^2$ and the surface area of the DBNCB equals $0.016\ m^2$. We have a weight gain of 42.21%, and from there, we conclude that there are greater fuel savings for the DBNCB. With A_t and A_e, the throat area and exit area are represented, respectively.

Table. 5 – Nozzle performance comparison for $NPR = 230$

	Dual Bell with Central Body Nozzle	E-D Nozzle
Area (m^2)	0.016	0.035
Length (mm)	97.40	177.56
Mach exit	4.60	2.76
Thrust (N)	143.98	103.22
Specific Impulse	57.71	41.37

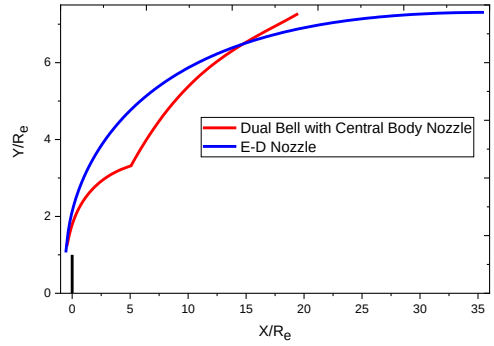

Fig. 27 – Shape of DBNCB and E-D nozzle the same $\frac{A_t}{A_e}$

In order to compare the efficiency, we compared the thrust of the two nozzles at different altitudes (different NPRs) see Fig. 28.

The NPR is gradually increased from 10 to 300. For each NPR result, the thrust of the two nozzles was determined.

The DBNCB is slightly superior to the E-D nozzle in terms of thrust when NPR≤30 and in the overexpansion mode, according to the results in the figure.

For NPRs ranging from 30 to 100 (low altitude mode), the thrust of the E-D nozzle exceeds that of the DBNCB by up to 25.82% for NPR=80.

When NPR≥100, there is a remarkable superiority in favor of the DBNCB in terms of thrust estimated at 32.15% of the maximum in the case NPR=260.

From there, we conclude that the DBNCB offers the best performance in most phases of flight.

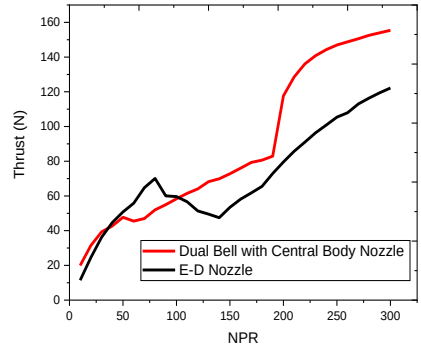

Fig. 28 – Comparison of Thrust

4. CONCLUSIONS

The main focus of this study is to utilize numerical methods in order to design profiles for a dual bell nozzle with a central body (DBNCB). The method was programmed in FORTRAN language. The basic nozzle chosen for this concept is an E-D nozzle. The obtained E-D nozzle performance (Mach, Pressure…) was compared to that of a plug nozzle. The study revealed that the E-D nozzle outperformed the Plug nozzle, as the former provided a 13% increase in thrust despite a 44.78% increase in weight compared to the latter. By conducting an inviscid simulation, we can compare the outcomes generated by our calculation code with those of a simulation. The calculated results are represented in different curves (pressure distributions and Mach number along the walls). This comparison gives a very good agreement, and the obtained results are very close. It is concluded that the two expansion waves are formed in the DBNCB. In conclusion, a k-ω SST turbulence model was used to conduct a comparative viscous calculation between the DBNCB and E-D nozzles, which have the same section ratio. The purpose of this study was to analyze how variations in nozzle pressure ratios (NPR) affect the mode of operation, and it was noted that, the results obtained for the DBNCB offer the best performance in most phases of flight.

REFERENCES

[1] M. Horn, and S. Fisher, *Dual-bell altitude compensating nozzles*, Pennsylvania State Univ., NASA Propulsion Engineering Research Center 2, 1993.
[2] K. Davis, E. Fortner, M. Heard, H. Mccallum and H. Putzke, Experimental and computational investigation of a dual-bell nozzle, *AIAA Paper 0377*.
[3] N. C. Génin and R. Stark, Experimental study on flow transition in dual bell nozzles, *Journal of Propulsion and Power*, Vol. **26**, no. 3, pp. 497-502, 2010.
[4] D. Schneider and C. Génin, Numerical investigation of flow transition behavior in cold flow dual-bell rocket nozzles, *Journal of Propulsion and Power*, Vol. **32**, no. 5, pp. 1212-1219, 2016.
[5] T. Hamitouche, M. Sellam, H. Kbab and S. Bergheul, Design and wall Fluid parameters evaluation of the dual-bell Nozzle, *International Journal of Engineering Research and Technology*, Vol. **12**, no. 7, pp. 1064-1074, 2019.
[6] D. Schneider, R. H. Stark, C. Genin, M. Oschwald and K. Kostyrkin, Operation mode transition of film-cooled dual-bell nozzles, *Joint Propulsion Conference*, Ohio, USA, 4467, 2018.
[7] A. Ferrero, E. Martelli, F. Nasuti and D. Pastrone, Fluidic control of transition in a dual-bell nozzle, *AIAA Paper 3788*.
[8] I. Bolgar, S. Scharnowski and J. C. Kähler, Effects of a Launcher's External Flow on a Dual-Bell Nozzle Flow, *Future Space-Transport-System Components under High Thermal and Mechanical Loads: Results from the DFG Collaborative Research Center TRR40*, pp. 115-127, 2021.
[9] H. Kbab, O. Abada and S. Haif, Numerical Investigation of Supersonic Flows on Innovative Nozzles (Dual Bell Nozzle), *Journal of Applied Fluid Mechanics*, Vol. **16**, no. 4, pp. 819-829, 2023.
[10] M. J. Zucrow and J. D. Hoffman, *Gas dynamics*, volume **2**-multidimensional flow, New York, 1977.
[11] C. C. Lee and D. Thompson, *Fortran program for plug nozzle desing*, NASA TM X-53019, 1964.
[12] H. Kbab, M. Sellam, T. Hamitouche, S. Bergheul and L. Lagab, Design and performance evaluation of a dual bell nozzle, *Acta Astronautica*, Vol. **130**, pp. 52-59, 2017.
[13] S. Haif, H. Kbab and A. Benkhedda, Design and Numerical Analysis of a Plug Nozzle, *Advances in Military Technology*, vol. **17**, no. 1, pp. 17-32, 2022.
[14] P. Reijasse, D. Coponet, J. M. Luyssen, V. Bar, S. Palerm, J. Oswald and P. Kuszla, Wall pressure and thrust of a dual bell nozzle in a cold gas facility, *Progress in Propulsion Physics*, Vol. **2**, pp. 655-674, 2011.